Structure of self-organized Fe clusters grown on Au(111) analyzed by grazing incidence x-ray diffraction

H. Bulou,[1,*] F. Scheurer,[1] P. Ohresser,[2] A. Barbier,[3] S. Stanescu,[4] and C. Quirós[4,†]

[1]*Institut de Physique et Chimie des Matériaux de Strasbourg, UMR 7504 CNRS-Université Louis Pasteur, 23 rue du Loess, Boîte Postale 43, F-67034 Strasbourg Cedex 2, France*

[2]*Laboratoire pour l'Utilisation du Rayonnement Electromagnétique, UMR 130 CNRS-Université Paris-Sud, Bâtiment 209 D, F-91898 Orsay Cedex, France*

[3]*CEA-Saclay DSM/DRECAM/SPCSI, F-91191 Gif-Sur-Yvette, France*

[4]*European Synchrotron Radiation Facility, Boîte Postale 220, F-38043 Grenoble Cedex, France*

(Received 3 September 2003; revised manuscript received 12 December 2003; published 14 April 2004)

We report a detailed investigation of the first stages of the growth of self-organized Fe clusters on the reconstructed Au(111) surface by grazing incidence x-ray diffraction. Below one monolayer coverage, the Fe clusters are in ''local epitaxy'' whereas the subsequent layers adopt first a strained fcc lattice and then a partly relaxed bcc(110) phase in a Kurdjumov-Sachs epitaxial relationship. The structural evolution is discussed in relation with the magnetic properties of the Fe clusters.

DOI: 10.1103/PhysRevB.69.155413 PACS number(s): 61.10.Nz, 68.55.Ac, 68.55.Jk

I. INTRODUCTION

Nanometer-sized objects such as metallic clusters or wires grown by controlled self-organization processes on surfaces exhibiting a defined strain field (e.g., reconstructed surfaces and patterned surfaces) are currently under extensive study. Because of the reduced dimensionality and the inflated importance of surface phenomena, these new objects exhibit original properties. In particular, they are models for investigating the magnetic properties of low dimensionality systems.[1–3] As a matter of fact, the magnetic properties are closely related to the intimate crystalline structure. Very small objects can present new and/or highly strained crystallographic phases with respect to the bulk equilibrium ones. These phases may in turn lead to peculiar spin phases or magnetic anisotropies. Investigating the structure of such small objects is therefore important but very difficult because of the very small amount of deposited material. Recently, the magnetic properties of self-organized Fe deposits on the reconstructed Au(111) surface were investigated by x-ray magnetic circular dichroism (XMCD). Three different spin phases were identified, as a function of coverage.[2] To fully understand these magnetic properties it is mandatory to precisely determine the crystalline structure of the Fe deposits. For such small clusters grown on a surface with a large lattice mismatch, one may expect strong differences compared to the bulk structure.

In this paper, the crystalline structure and strain relaxation of Fe deposits on Au(111) are investigated by grazing incidence x-ray diffraction (GIXD) as a function of Fe coverage. In a first part, the characteristics of the reconstructed Au(111) surface are given, and the reciprocal lattice is analyzed by GIXD. In a second part, the structure of Fe deposits is studied as a function of coverage, from isolated clusters to several monolayers (ML). It is shown that Fe clusters first grow in close registry on the highly inhomogeneous reconstructed Au(111) surface. Slight changes appear in the Fe-Fe distances first at a one-dimensional coalescence, then a relaxation starts upon the growth of the second layer. Above 3 ML, the film undergoes a phase transition from a fcc(111) phase to a bcc(110) phase.

II. EXPERIMENT

The experiments were performed in ultrahigh vacuum conditions on the surface diffraction beamline (ID3) at the ESRF on a *z*-axis diffractometer.[4,5] The single crystalline Au substrate is of (111) orientation within $\pm 0.1°$. It is prepared *in situ* by Ar^+ sputtering and annealing cycles, up to 1000 K. After treatment, the mosaicity of the Au sample is negligible (below $\sim 0.01°$) and the diffracting domain size as large as 1800 Å, as determined from rocking scans. The Fe is evaporated from a high-purity rod, heated by electron bombardment in an evaporation cell equipped with a flux monitor. During the evaporation the pressure lies in the low 10^{-10} mbar range. The growth is made with the substrate held at room temperature. After each analyzed coverage, the sample is cleaned and the Fe deposition repeated. The thickness of the deposit is controlled by fitting the specular reflectivity Kiessig fringes. The surface and Fe deposits cleanliness are controlled by Auger electron spectroscopy. The (111) single crystalline surface is described by a triangular unit cell[6,7] defined by the surface in-plane basis vectors $\vec{a}_1$, $\vec{a}_2$, making a 120° angle ($a_1 = a_2 = a_0/\sqrt{2}$, where $a_0 = 4.07$ Å is the fcc bulk parameter of gold) and $\vec{a}_3$, perpendicular to the surface ($a_3 = \sqrt{3} a_0$). The reciprocal space indices h and k describe the in-surface plane momentum transfer, and l the perpendicular to the surface momentum transfer. The units of the reciprocal lattice are $|\vec{H}| = |\vec{K}| = 4\pi/\sqrt{3} a_1 = 2.52$ Å^{-1} for wave-vector transfers parallel to the surface and $|\vec{L}| = 2\pi/\sqrt{3} a_0 = 0.89$ Å^{-1} for positions along the surface normal direction. The photon energy is set to 17.176 keV to obtain high flux and access to large momentum transfer values. The angular resolution for in-plane scans is 0.5 μrad and the incidence angle tuned close to the value for total

external reflection of the x-rays [$\sim 0.3°$ at 17.176 keV for Au(111)].

III. Au(111) SURFACE RECONSTRUCTION

In order to understand the modifications in the x-ray-diffraction scans induced by the evaporation of very small amounts of Fe it is important to first precisely describe the Au(111) reciprocal lattice. The strong relativistic effects experienced by the electrons in gold produce a large mismatch between the bulk equilibrium interatomic distance and the surface one.[8,9] Moreover, since the chemical nature of the surface and bulk atoms is the same, the interactions between two surface atoms and between a surface and a bulk atom have approximately the same magnitude. Hence, for the surface atoms, a competition results between the trend to get closer, or to adopt the bulk equilibrium distance. In the case of the Au(111) surface, the most favorable energetic situation consists of a surface split into domains of two different types: domains where the interatomic distance is the one of an ideal gold surface (hcp stacking) and domains with the bulk interatomic distance (fcc stacking). The two types of domains are separated by discommensuration lines, several atomic distances wide, which make the junction between the hcp and the fcc domains. The interatomic distances between surface atoms are very inhomogeneous since they vary from 2.65 Å to 2.86 Å.[9] The periodic succession of parallel fcc and hcp stripe domains along the denser $\langle \bar{1}01 \rangle$ atomic direction forms an uniaxial $22\times\sqrt{3}$ reconstruction. The density increase along $\langle \bar{1}01 \rangle$ rows (by introducing one additional Au atom every 22 bulk atoms) produces stress in the other symmetry equivalent directions [Au(111) belongs to the $Fm3m$ space group]. Hence the stripe domain reconstruction is unstable for large areas[10,11] and the best compromise is the formation of three types of stripe domain reconstructions, each of them associated with one of the three equivalent $\langle \bar{1}01 \rangle$ directions. The intersection between the discommensuration lines of the different stripe domains induces the formation of kinks. The kinks are themselves ordered, and this leads to a structure in which two of three possible rotational equivalent domains of the stripe domain structure alternate periodically across the surface, forming the well-known zigzag pattern.[6,12,13]

In summary, the herringbone-reconstructed Au(111) surface can be understood as the superposition of three different lattices [Fig. 1(a)].

(1) The fcc bulk lattice with lattice parameter a_0.

(2) The surface reconstruction lattice, used to be called $22\times\sqrt{3}$, which is the consequence of the density increase along the $\langle \bar{1}01 \rangle$ rows. In a $\langle \bar{1}01 \rangle$ direction there is a $22a_0$ superperiodicity, whereas in the perpendicular $\langle 1\bar{2}1 \rangle$ direction, the superperiodicity is $\sqrt{3}a_0$.

(3) The rectangular $(\lambda\times\Lambda)$ kink superlattice with $\lambda = 7.2$ nm (fixed precisely by the $22a_0$ reconstruction periodicity), and Λ varying typically between 15 nm and 50 nm. The length Λ experiences very large fluctuations from one sample to another, depending on the preparation conditions and the density of defects in the crystal.[14]

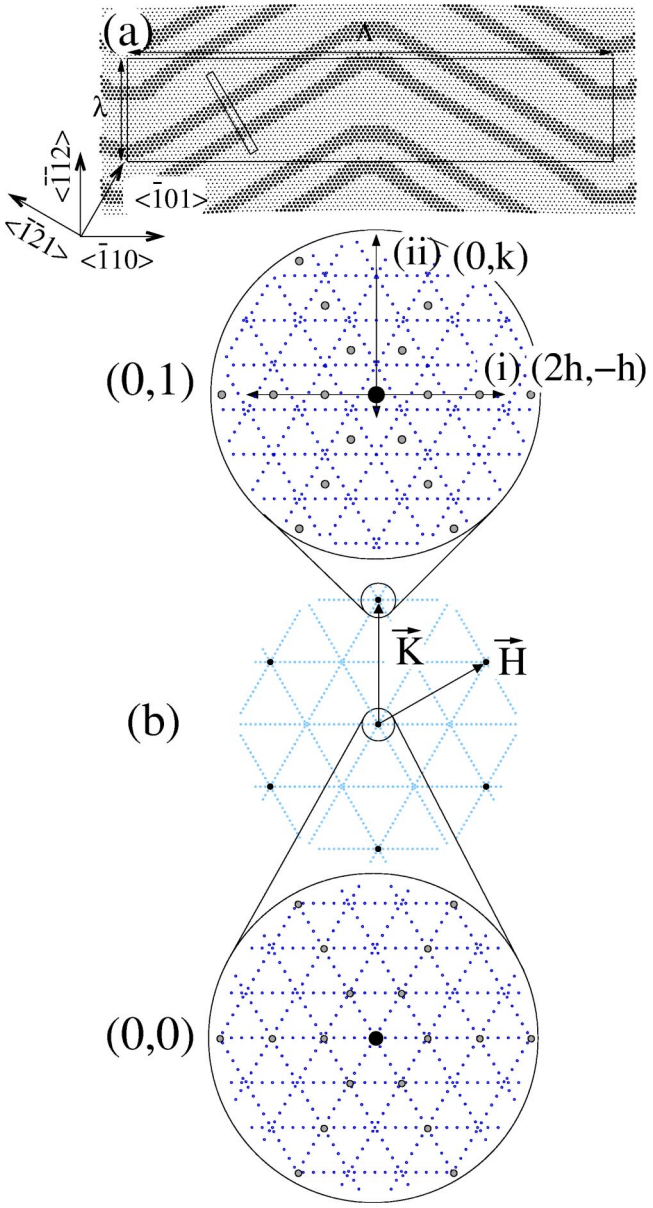

FIG. 1. (a) Reconstructed Au(111) surface as simulated by molecular dynamics (Ref. 9). The $22\times\sqrt{3}$ reconstruction cell is represented (small rectangle), as well as the rectangular herringbone unit cell (large rectangle). In this simulation the large periodicity of the kink array is $\Lambda = 32$ nm (see text). (b) Reciprocal surface lattice of reconstructed Au(111) (middle) with enlargements around the (0,0) (bottom) and (0,1) (top) reflections. The intersection of the crystal truncation rods with the surface plane are represented by the dark disks, the $22\times\sqrt{3}$ reconstruction by smaller gray disks and the reflections due to the kink lattice by dots (for the sake of clarity, the contribution of the kinks is only represented in the enlarged regions). The different types of GIXD scans recorded in the present study are indicated by arrows as (i) and (ii).

The resulting Au(111) reciprocal space is made of the superposition of the reciprocal lattices of the three different lattices and the symmetry-equivalent domains, as represented in Fig. 1(b) in the $\vec{H}$, $\vec{K}$, $\vec{L}$ basis. The larger dark disks are the intersections with the $(\vec{H},\vec{K})$ plane of the crystal trunca-

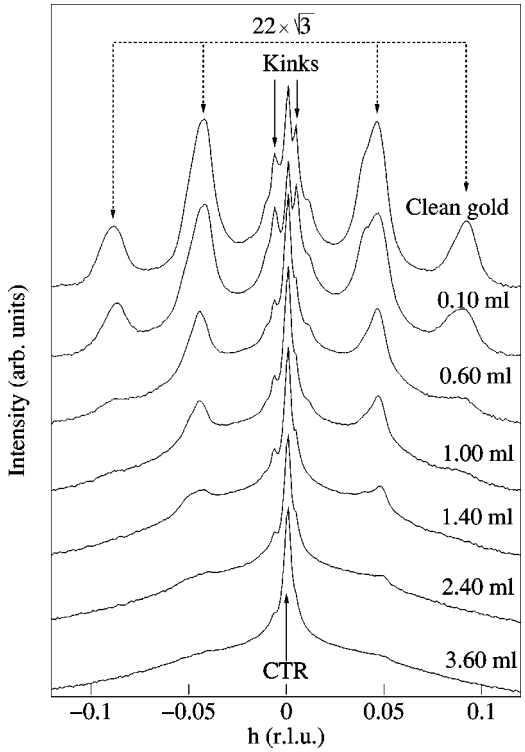

FIG. 2. Selected in-surface-plane HK scan along $(2h, -h)$ across the (0 1 l) rod at $l=0.12$ for clean gold (top) and for several Fe deposits. The features of the $22\times\sqrt{3}$ reconstruction are indicated, as well as the small structures induced by the projections of the kink lattice reflections (see text).

tion rods (CTR),[15] the small gray disks represent the lattice of the $22\times\sqrt{3}$ reconstruction, and the dots represent the theoretical lattice formed by the regular arrangement of the kinks.

The Au(111) surface reconstruction has already been investigated in detail by GIXD with a high angular resolution by Sandy *et al.*[6] Note, however, that the reciprocal space represented in Fig. 6 of Ref. 6 is in fact only valid around the specular reflection: since the rectangular lattice is incommensurate, one does not have exactly the same positions of the kink reflections around a (0 1 l) CTR [see Fig. 1(b)]. Indeed, the representation of our Fig. 1(b) corresponds much better to the experimental scans of Sandy *et al.* (Fig. 8 of Ref. 6).

Figure 2 shows a scan in the $(2h, -h)$ direction [labeled (i) in Fig. 1(b)] on clean Au(111). The gold (0 1 l) CTR, located in central position, is surrounded on both sides by two intense satellite peaks which exactly correspond to the 1/22 periodicity of the reconstruction. In addition, several faint structures appear close to the (0 1 l) CTR, and possibly near the first-order reconstruction peaks. These faint structures are actually the projections of the kink lattice superstructure reflections [small dots in the top panel of Fig. 1(b)]. From this scan alone it is not possible to precisely determine the Λ periodicity of the kink lattice since due to the finite resolution function the position of the projection of the peak is depending on its intensity, which is not known *a priori*. To determine Λ a specific mapping is needed, which is out of the scope of this paper (see Ref. 6 for this point).

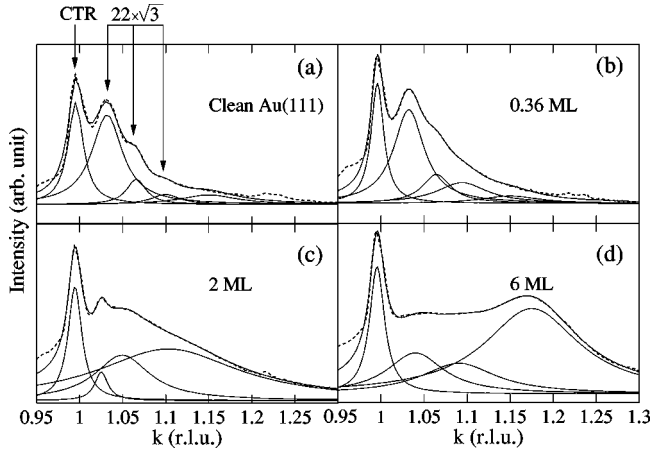

FIG. 3. K scan along the (k, 0, 0.12) direction with respect to the Fe thickness. (a) For the clean Au(111) surface. The first peak at $k=1$ corresponds to the intersection of the crystal truncation rod (CTR) with the surface plane, the second and following are the different orders of the reconstruction. (b) For 0.36 ML Fe, (c) for 2.0 ML and (d) for 6.0 ML. Note that the small bump at $k\approx 1.225$ is always present on clean gold and likely belongs to a residual disoriented crystallite.

In Fig. 3(a), representing a K scan at $h=0$ and $l=0.12$ [referenced as (ii) in Fig. 1(b)] for clean gold, one can identify several features: the Au crystal truncation rod ($k=1$), and the projection on the $[h=0]$ direction of the first, second, and third orders of the $22\times\sqrt{3}$ reconstruction. These reconstruction peaks give a projected distance of 2.78 Å, which indeed corresponds to the average surface parameter of a $\sim 4\%$ over close-packed Au(111) surface layer. Due to the strong interatomic distance inhomogeneity, the contributions are rather broad, and it is difficult to quantitatively determine the modifications of the x-ray-diffraction scans upon Fe deposition at very low coverage. The K scans were therefore fitted by different Lorentzian contributions.[6] For clean gold, the K scan was simulated by the superposition of five peaks [Fig. 3(a)], accounting for the Au crystal truncation rod, for the first, second, and third order peaks of the $22\times\sqrt{3}$ reconstruction. The fifth peak was added to take into account globaly the higher orders. The positions of the different orders of the gold reconstruction peaks were unambiguously determined from the HK scans in Fig. 2. We verified, however, that taking the peak positions as free fit parameters, the fit procedure ends up with the good positions. One can notice the good agreement between the fit and the experimental data.

IV. Fe DEPOSITION

It is well known that the kink positions of the herringbone reconstruction act as preferential nucleation sites for most $3d$ metals.[16–20] In the case of Fe, this leads to the growth of monolayer-high clusters, located at the kinks, expanding laterally with increasing coverage.[17]

Upon Fe deposition, the main effect is the reduction of the intensity of the reconstruction peaks (Fig. 2). At about 0.5 ML, the second-order peak has nearly vanished. The first-

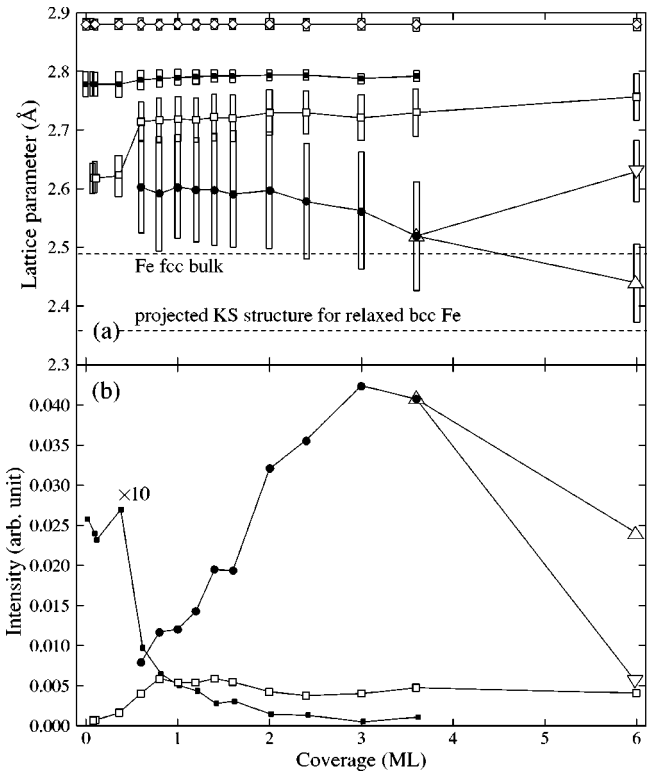

FIG. 4. (a) Real space distances derived from the different contributions deduced from the fits of the *K* scans (Fig. 3) as a function of the Fe coverage. The error on the peak positions is ~0.5% (about the symbol size). The open bars represent the widths of the different contributions. (b) Intensity of the corresponding fcc and bcc Fe contributions. (◇) represent the bulk gold, (■) the gold surface reconstruction, (□) the pseudomorphic fcc Fe, (●) the relaxed fcc Fe. The open triangles stand for the bcc Fe (see text for details). The positions of the bulk fcc and the projected bcc iron are indicated by dashed lines.

order reconstruction peak can, however, be observed up to about 2 ML [Fig. 4(b)]. This means that the reconstruction is progressively lifted, but the surface is still over close-packed since the first-order peak remains. Interestingly, the features due to the rectangular kink lattice remain present. Intuitively one would argue that these features can only be present if there is a $22\times\sqrt{3}$ reconstruction. Since they do not disappear together with the reconstruction, one must assume that the Fe clusters nucleated at the kinks somehow help the Au substrate to keep the memory of the rectangular lattice. A possible mechanism would be the introduction of a periodic strain field in the gold substrate during the growth. A similar mechanism has indeed been proved recently in the case of N/Cu(100) (Ref. 21) and was also suggested by grazing incidence small angle x-ray scattering experiments performed on self-organized Co/Au(111) clusters.[14]

The positions, widths, and intensities of the CTR and the first-order satellite peak of the reconstruction can be determined with a good accuracy on both *HK* (Fig. 2) and *K* scans (Fig. 3), all along Fe deposition up to about 2.5 ML (Fig. 4). Importantly, one can notice that the positions of the CTR and first reconstruction peaks do not change with increasing coverage, and the widths remain nearly constant (Fig. 4). The reconstruction periodicity is therefore not affected by the Fe deposition and the CTR and first satellite parameters can be easily determined by the fit procedure for all Fe coverages. Upon Fe growth, the second and next orders of the reconstruction peaks disappear (this is clearly demonstrated by the *HK* scans in Fig. 2) and are progressively replaced in the *K* scans by a first and then a second contribution (Fig. 2). The width of these new contributions is much larger than the typical widths obtained for the satellite peaks of clean Au(111) [Fig. 4(a)]. The larger width is due to a reduced diffracting domain size of Fe islands, and/or to an enhanced parameter spreading with respect to clean gold. Due to the large width of the contributions, the analysis of the *K* scan in the (0 2 *l*) CTR region unfortunately does not allow to discriminate the two effects, but the spreading effect seems dominant. An upper limit of the spreading is therefore given by the bars in Fig. 4(a). Below 1 ML there are only slight modifications in the *K* scan, indicating that the Fe atoms grow in near registry with the underlying gold atoms. This growth phase is therefore qualified as fcc. From the fits, one can locate more precisely the different contributions [Fig. 4(a)]. The first contribution attributed to fcc Fe (□) shows a slight and sudden increase of the lattice parameter around 0.4 ML, from about 2.62 Å to ~2.72 Å before staying more or less constant with increasing thickness. The jump is significantly larger than the error in the position determination and even than the width due to the parameter spreading (~0.08 Å). Between 0.6 ML and 3 ML a second contribution (●) appears with a slightly smaller parameter.

Above 3 ML, the latter contribution splits progressively into two intense contributions (△,▽), which correspond to a phase transition towards the stable bulk Fe bcc(110) phase. The epitaxial relationship corresponds to an intermediate orientation between the Kurdjumov-Sachs (KS) and the Nishiyama-Wassermann (NW) orientations [Fig. 5(a)]. Since the global symmetry corresponds to the KS symmetry, we will refer to this particular orientation as KS. Diffracted intensity maps around (0 1 0.12) and (0 1 1.7) at constant *l* show indeed typical patterns, although fuzzy, for such an orientation [Fig. 5(b)] (see Ref. 22 and references therein). Simulations of the peak positions in the reciprocal space reproduce the experimental data rather well (see Discussion). This structure induces a projected contribution in the *K* scan at about (0.05 1.17 0.12).

V. DISCUSSION

From the results above, one immediately notices that the crystalline structure of the Fe clusters evolves as a function of coverage. The individual contributions in the diffraction scans deserve to be discussed separately.

The first Fe contribution (□) in Fig. 4(b) exhibits a linear intensity increase with the Fe thickness and then becomes constant after ~1 ML. Its average lattice parameter varies from ~2.62 Å to 2.72 Å and then remains almost constant. This behavior results from the competition between the Fe-Fe and Au-Fe interactions. The Fe-Fe interactions tend to favor small Fe-Fe interatomic distances. Moreover, in the case of clusters, the edge atoms emphasize this effect.[23] Con-

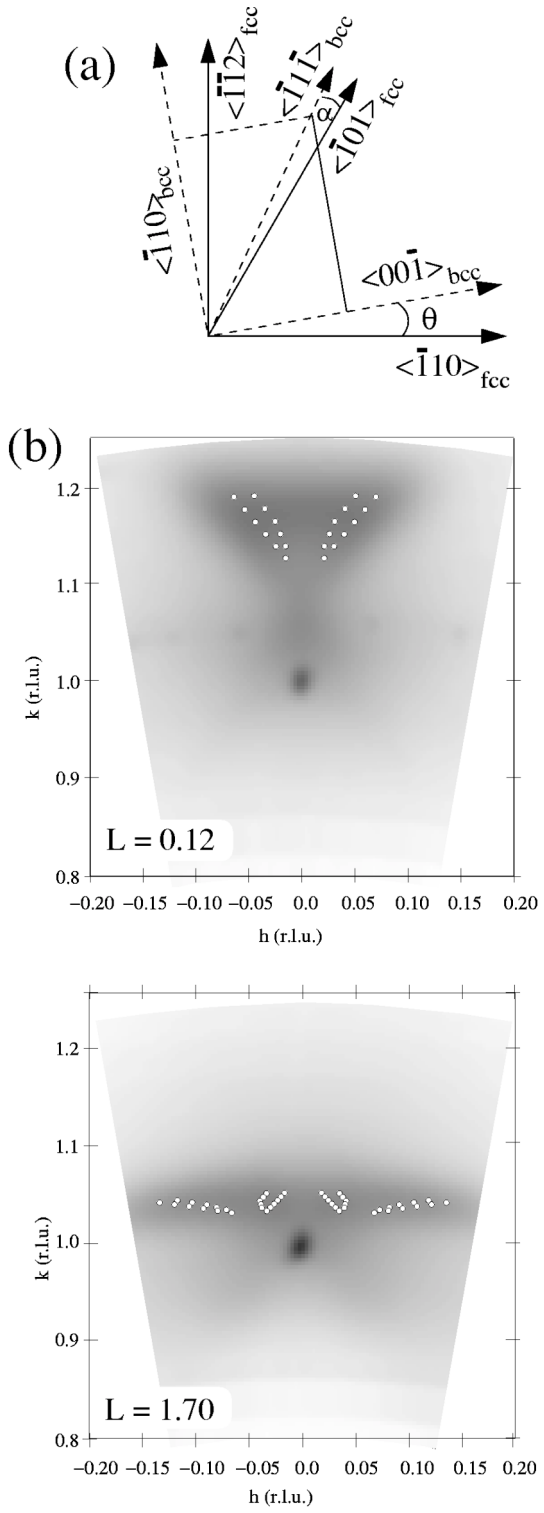

FIG. 5. (a) bcc(110) lattice orientation with respect to the fcc(111) substrate for the Nishiyama-Wassermann ($\theta=0$) and Kurdjumov-Sachs ($\alpha=0$) orientations (the spots are originating from, respectively, three and six types of symmetry equivalent domains). (b) Maps around the ($h\ k\ l$)=(0 1 0.12) and ($h\ k\ l$) =(0 1 1.7) regions of the reciprocal space for 6.0 ML Fe. Simulated reflections (white dots) for a spread of parameters and θ angles are superimposed. They give an indication of the rotational and parametric disorders.

versely, the Au-Fe interactions tend to impose an iron registry growth, as can be inferred from the weak modifications of the K scans. In the 0–0.4 ML thickness range, the nucleation takes place on the kinks, where the interatomic distances are the smallest [2.60–2.65 Å (Ref. 9)]. This corresponds indeed to the peak position of the first fcc Fe contribution (□).

While growing laterally upon increasing the coverage, the clusters expand over the hcp or fcc regions where the gold atoms are separated by 2.80–2.85 Å, what leads to an increased mismatch. The one-dimensional (1D) coalescence ($\sim$0.4 ML) of adjacent islands along $\langle\overline{112}\rangle$ directions produces a sudden loss of edge atoms. This latter effect, associated with the large mismatch between Fe and Au enhances the weight of Fe-Au interactions and probably leads to the observed transition at this coverage.

The second fcc Fe phase [(●) in Fig. 4(b)] with a slightly smaller lattice parameter starts growing between 0.6 ML and 3 ML. The intensity increase is proportional to the additional Fe thickness, showing that all incoming Fe atoms adopt this crystallographic configuration. This is consistent with the onset of the growth of a second Fe layer, with a slightly relaxed parameter on top of the first epitaxial Fe layer: indeed, the onset of the second layer growth starts between 0.5 and 0.8 ML as noticed by scanning tunnel microscopy experiments.[17] In this thickness range (0.6–3 ML) the Fe film must be understood as a partly relaxed Fe fcc layer on an interfacial pseudomorphic layer.

Above 3–4 ML, the strain in the Fe layer starts to relax through a progressive transformation into the bcc Fe phase with the KS bcc(110)$\|$fcc(111) epitaxial relationship. Indeed, this epitaxy does not yield any Bragg position along our K scans (Fig. 3) and the contribution observed at $k \approx 1.17$ is only due to the tail of the bcc Bragg peaks located outside the K scan. This interpretation fairly well explains the decrease, and finally splitting into two distinct bcc (△,▽) contributions of the fcc (●) signal in Fig. 4(b). The (△) contribution corresponds to the projection of the KS structures, observed in Fig. 5(b), in the $\vec{K}$ direction. The (▽) feature results from the crossing of the two KS structures on the $\vec{K}$ axis. At large coverage the Fe film consists of a bcc layer on top of an interfacial pseudomorphic 1 ML thick fcc layer. It is interesting to note that the fcc to bcc transition occurs once the fcc lattice parameter has reached the value adopted by the bulk γ-Fe phase. The somewhat fuzzy diffraction patterns in Fig. 5(b) are due to both rotational disorder in the θ angle [as defined in Fig. 5(a)] and to a parametric spreading in the bcc $\langle\overline{1}10\rangle$ direction, from about 2.50 Å to 2.65 Å. For the highly strained domains, the orientation is rather NW ($\theta\approx 0$), with nearly no orientational disorder, whereas for the less strained domains, θ corresponds roughly to half of the ideal angle expected for the KS orientation, with an angular distribution of about 1°. This can be seen in Fig. 5 where the reflections for different orientations and parameters are superimposed to the experimental maps.

VI. CONCLUSION

The structure and growth of Fe deposits on reconstructed Au(111) have been investigated by GIXD. Up to one mono-

layer, Fe grows in close registry with the reconstructed Au(111) substrate. However, due to the great inhomogeneity of the gold interatomic distances at the surface, slight changes in the in-plane atomic distances already occur during the lateral expansion of the monolayer-high Fe clusters upon growth. We qualify the structure as ''local pseudomorphism.'' Below the 1D coalescence, the in-plane parameter of the Fe islands is expanded with respect to its metastable bulk phase (2.62 Å), and after the coalescence along $\langle\overline{1}12\rangle$, it is even more expanded (2.72 Å). Upon the second Fe layer growth, the parameter relaxes towards smaller values (2.50–2.60 Å). Above 3 ML the film transits progressively and breaks into partly relaxed bcc(110) domains, in an orientation intermediate between the Kurdjumov-Sachs and Nishiyama-Wassermann epitaxial relationships. These structural results are consistent with the XMCD observations[2] where strong changes in the magnetic properties were evidenced. In particular, the magnetic spin moment showed a sharp increase at the unidimensional coalescence around 0.4 ML (going from $\sim 1.4\mu_B$ to $\sim 2.4\mu_B$). This change can now be correlated to the increase of the lattice parameter. Indeed, it is well known that for fcc Fe magnetism and structure are linked with, in particular, a tendency to high magnetic spin values for larger atomic volume. Moreover, to fit the evolution of the magnetic anisotropy energy with the coverage a Néel model was used in Ref. 2 assuming a pseudomorphic growth of the first Fe layer. This assumption is now further experimentally confirmed by the present GIXD results.

ACKNOWLEDGMENTS

The authors are pleased to acknowledge the ID03 beamline staff of the ESRF for excellent experimental conditions and support during these experiments. We would also like to thank O. Fruchart for a fruitful discussion and A. Tagliaferri for his technical help.

*Electronic address: bulou@ipcms.u-strasbg.fr
†Present address: Depto. de Física, Universidad de Oviedo, Av. Calvo Sotelo s/n, 33007 Oviedo, Spain.

[1] P. Gambardella, A. Dallmeyer, K. Malti, M.C. Malagoli, W. Eberhardt, K. Kern, and C. Carbone, Nature (London) **416**, 301 (2002).
[2] P. Ohresser, N.B. Brookes, S. Padovani, F. Scheurer, and H. Bulou, Phys. Rev. B **64**, 104429 (2001).
[3] J. Shen, J.P. Pierce, E.W. Plummer, and J. Kirschner, J. Phys.: Condens. Matter **15**, R1 (2003).
[4] S. Ferrer and F. Comin, Rev. Sci. Instrum. **66**, 1674 (1995).
[5] http://www.esrf.fr
[6] A.R. Sandy, S.G.J. Mochrie, D.M. Zehner, K.G. Huang, and D. Gibbs, Phys. Rev. B **43**, 4667 (1991).
[7] G. Grübel, K. Huang, Doon Gibbs, D.M. Zehner, A.R. Sandy, and S.G.J. Mochrie, Phys. Rev. B **48**, 18 119 (1993).
[8] J. Ferreirinho, R. Ruffini, and L. Stella, Phys. Lett. **91B**, 314 (1980).
[9] H. Bulou, and C. Goyhenex, Phys. Rev. B **65**, 045407 (2002).
[10] V.I. Marchenko, Zh. Éksp. Theor. Fiz. **81**, 1141 (1981) [Sov. Phys. JETP **54**, 605 (1981)].
[11] O.L. Alerhand, D. Vanderbilt, R.D. Meade, and J.D. Joannopoulos, Phys. Rev. Lett. **61**, 1973 (1988).
[12] J.V. Barth, H. Brune, G. Ertl, and R.J. Behm, Phys. Rev. B **42**, 9307 (1990).
[13] S. Narasimhan and D. Vanderbilt, Phys. Rev. Lett. **69**, 2455 (1992).
[14] O. Fruchart, G. Renaud, A. Barbier, M. Noblet, O. Ulrich, J.-P. Deville, F. Scheurer, J. Mane-Mane, V. Repain, G. Baudot, and S. Rousset, Europhys. Lett. **63**, 275 (2003).
[15] I.K. Robinson, Phys. Rev. B **33**, 3830 (1986).
[16] B. Voigtländer, G. Meyer, and N.M. Amer, Phys. Rev. B **44**, 10 354 (1991); Surf. Sci. **255**, L529 (1991).
[17] J.A. Stroscio, D.T. Pierce, R.A. Dragoset, and P.N. First, J. Vac. Sci. Technol. A **10**, 1981 (1992).
[18] D.D. Chambliss, R.J. Wilson, and S. Chiang, Phys. Rev. Lett. **66**, 1721 (1991).
[19] J.A. Meyer, J.D. Baikie, E. Kopatzki, and R.J. Behm, Surf. Sci. **365**, L647 (1996).
[20] M. Fonin, Y.U. Dedkov, U. Rüdiger, and G. Güntherodt, Surf. Sci. **529**, L275 (2003).
[21] B. Croset, Y. Girard, G. Prévot, M. Sotto, Y. Garreau, R. Pinchaux, and M. Sauvage-Simkin, Phys. Rev. Lett. **88**, 056103 (2002).
[22] S. Boukari, E. Beaurepaire, H. Bulou, B. Carrière, J.P. Deville, F. Scheurer, R. Baudoing-Savois, and M. De Santis, Surf. Sci. **430**, 37 (1999).
[23] V.S. Stepanyuk, D.I. Bazhanov, A.N. Baranov, W. Hergert, P.H. Dederichs, and J. Kirschner, Phys. Rev. B **62**, 15 398 (2000).